lubricants

MDPI

Article

Effect of Cr Doping Content on the Mechanical and Tribological Properties of Cr-C/DLC Films on ACM Rubber Surfaces

Kanghai Chen [1,2], Nini Zhen [1,2], Huatang Cao [3,*], Qiaoyuan Deng [1,*] and Feng Wen [4,*]

[1] State Key Laboratory of Tropic Ocean Engineering Materials and Materials Evaluation, Special Glass Key Laboratory of Hainan Province, Hainan University, Haikou 570228, China; 23210805000020@hainanu.edu.cn (K.C.); 14797339669@163.com (N.Z.)
[2] School of Materials Science and Engineering, Hainan University, Haikou 570228, China
[3] State Key Laboratory of Materials Processing and Die & Mould Technology, School of Materials Science and Engineering, Huazhong University of Science and Technology, Wuhan 430074, China
[4] Hunan Provincial Key Laboratory of Fine Ceramics and Powder Materials, School of Materials and Environmental Engineering, Hunan University of Humanities, Science and Technology, Loudi 417000, China
* Correspondence: caoht@hust.edu.cn (H.C.); qydeng@hainanu.edu.cn (Q.D.); fwen323@163.com (F.W.)

Abstract

Recently, diamond-like carbon (DLC) films have been considered for enhancing the wear resistance of rubber because rubber exhibits a high coefficient of friction and is prone to wearing out. However, the significant difference in thermal expansion coefficients between DLC films and rubber often leads to high residual stresses and poor interfacial adhesion, which limits their application in dynamic seals. In this study, Cr-C/DLC composite films were prepared using magnetron sputtering, and the effects of varying Cr contents (0.8 at.%, 1.4 at.%, 4.3 at.%, and 7.0 at.%) on interfacial adhesion and tribological properties were investigated. Scanning electron microscopy (SEM) analysis revealed no distinct demarcation lines in the composite films, indicating strong adhesion to the substrate. X-ray photoelectron spectroscopy (XPS) analysis revealed that chromium doping promoted the conversion of sp^3 bonds to sp^2 bonds. Adhesion and tribology tests revealed that introducing a Cr-C layer with higher Cr content within the range of 0.8 at.% to 7.0 at.% enhanced the film's adhesion, reducing the CoF value of the composite film to 0.13–0.14. Specifically, the RF80 sample (4.3 at.% Cr) exhibited excellent interfacial adhesion and optimal tribological performance, with a CoF value reduced to 0.13 and wear rate of 3.1×10^{-4} $mm^3/(Nm)$. In summary, modulating the Cr doping content can significantly enhance the interfacial adhesion strength and tribological properties of Cr-C/DLC composite films on rubber surfaces, providing an effective solution for optimizing rubber seals.

Keywords: Cr-C interlayer; diamond-like carbon film; tribology; mechanical properties

Check for updates

Received: 9 March 2026
Revised: 30 March 2026
Accepted: 30 March 2026
Published: 31 March 2026

Copyright: © 2026 by the authors. Licensee MDPI, Basel, Switzerland. This article is an open access article distributed under the terms and conditions of the Creative Commons Attribution (CC BY) license.

1. Introduction

Acrylic rubber (ACM) is an elastomer primarily copolymerized from acrylic monomers, exhibiting outstanding resistance to aging, thermal oils, high temperatures, and ozone [1,2]. Due to these exceptional properties, ACM is widely used in seals, O-rings, hoses, gaskets, and other components, particularly in high-temperature and oil-resistant environments [3,4]. Rubber dynamic seals undergo compressive deformation during operation and often exhibit very high friction when interacting with other engineering materials, leading to rubber wear failure. This limits the service life of rubber seals. Diamond-like carbon (DLC) films exhibit high hardness, low friction coefficients, and excellent chemical

and thermal stability [5–7], and are widely used in cutting tools, hydraulic components, and automotive parts [8,9]. DLC films have emerged as an ideal choice for enhancing the wear resistance of rubber. However, due to the significant difference in thermal expansion coefficients between DLC (1.18–1.8 $\times$ 10^{-6} K^{-1}) and ACM rubber (approximately 100 $\times$ 10^{-6} K^{-1}) [10,11], the deposition process tends to generate high residual stresses, leading to insufficient film adhesion [12].

Numerous studies have investigated the interfacial adhesion strength of DLC films on rubber surfaces. Plasma pretreatment is performed before DLC film deposition to clean and activate the surface, thereby enhancing adhesion between the rubber and the film [13]. Martinez-Martinez et al. [14] subjected the substrate to 30–40 min of Ar plasma etching before deposition, followed by treatment with an Ar/H_2 composite plasma, which improved the bond strength between ACM rubber and DLC films. Pei et al. [15] found that after W-doping DLC films, both fluoroelastomer (FKM) and nitrile butadiene rubber (NBR) exhibited excellent adhesion. Additionally, introducing an intermediate layer between the substrate and the film can further enhance interfacial bonding strength. Lubwama et al. [16] deposited DLC and Si-DLC coatings with and without Si-C interlayers on nitrile rubber. The results showed that coatings with Si-C interlayers had improved adhesion, exhibiting an adhesion strength of 4A. He et al. [17] deposited DLC films with varying Ti interlayer thicknesses on the surface of HNBR rubber. The study found that increasing the thickness of the Ti interlayer reduced the internal stress of the DLC film. Moreover, as the Ti interlayer served as a load-bearing layer, the co-deformation ability between the film and the rubber was enhanced, reducing the risk of film failure during friction. In addition, Xu et al. [10] discovered that by adding a Cr/Cr-C sublayer between stainless steel and the DLC film and a adjusting its thickness, the stress concentration of the film was decreased. Furthermore, the formation of this nanocomposite sublayer enhanced crack propagation resistance, thus improving the film's adhesion and wear resistance. The above literature confirms the great potential of introducing an interlayer to reduce film stress, enhancing the adhesion between the film and the substrate (either a hard substrate or a rubber substrate), and improving tribological properties. Chromium (Cr) has excellent compatibility with the matrix and readily reacts with carbon, effectively reducing the residual stress in the film, contributing to enhancing the bonding strength between the film and the rubber matrix. Additionally, introducing a Cr-C interlayer helps mitigate the significant difference in thermal expansion coefficients between DLC and the rubber matrix. However, most studies focus on the impact of the presence or thickness of the interlayer on the adhesion and tribological properties of DLC films on rubber surfaces. Few studies have reported the impact of the doping atom content in the interlayer on the microstructure, mechanical properties, and tribological properties of DLC films on rubber surfaces.

This study aims to explore the influence of the Cr-C interlayer on the structure and properties of DLC films on ACM rubber surfaces. In this study, Cr-C serves as the interlayer, and the effects of interlayers with varying Cr doping levels on adhesion between the film and the rubber matrix and their tribological properties are investigated. This research has significant scientific value in further enriching the study of DLC films on rubber surfaces and practical implications for expanding the applications of ACM rubber.

2. Materials and Methods

2.1. Deposition of Films

The film was deposited on ACM rubber (15 mm $\times$ 15 mm $\times$ 3 mm) using magnetron sputtering. First, the ACM rubber was placed in a beaker containing deionized water and boiled for 5 min to remove grease contaminants from the rubber surface. Subsequently, the rubber was ultrasonically cleaned in anhydrous ethanol for 15 min. This cleaning process

was repeated multiple times until the ACM rubber was completely clean. Finally, the cleaned rubber was dried in an oven at 50 °C for 30 min to remove surface moisture.

To prepare for subsequent thin-film deposition and performance testing, a single-crystal silicon wafer (100) measuring 20 mm × 10 mm × 0.5 mm was pretreated. Prior to deposition, a rigorous cleaning procedure was strictly followed to ensure surface cleanliness: the wafer was placed in a beaker containing anhydrous ethanol and subjected to ultrasonic agitation for at least 15 min. During cleaning, direct contact with the wafer surface using tweezers or other tools was avoided to prevent scratches or contamination. This ultrasonic cleaning process was repeated three times, with fresh anhydrous ethanol replaced each cycle to ensure complete removal of oils, particles, and other impurities from the wafer surface.

After cleaning the rubber substrate and silicon wafers, co-sputtering with Cr and graphite targets was employed to prepare a Cr-C intermediate layer. The Cr target was powered by an RF power supply (RF-MS) with power levels adjusted to four gradients: 40, 60, 80, and 100 W. The graphite target was deposited using high-power pulsed magnetron sputtering (HiPIMS), with the HiPIMS voltage set at 700 V, a duty cycle of 2%, and a frequency of 0.2 kHz. During deposition, the substrate was subjected to a pulsed bias of −150 V at a frequency of 40 kHz and a duty cycle of 75%, with the working gas pressure maintained at 1.5 Pa. All top-layer DLC films were deposited using HiPIMS with constant parameters to ensure sample consistency: a pulsed bias of −150 V was applied to the substrate, HiPIMS voltage was set at 700 V, duty cycle at 2%, frequency at 0.2 kHz, and deposition time at 1 h. The deposition parameters of the Cr-C/DLC films and the doping content of Cr in the Cr-C interlayer are presented in Table 1.

Table 1. Deposition parameters for the Cr-C intermediate layer and DLC film, and Cr doping content in the interlayer.

Sample	Interlayer				Top-Layer		Bias	Working Pressure
	C Target HiPIMS Power	Cr Target RF Power	Deposition Time	Cr Doping Content	C Target HiPIMS Power	Deposition Time		
RF40	700 V/2%/ 0.8 kHz	40 W	30 min	0.8 at.%	700 V/2%/ 0.8 kHz	60 min	−150 V/75%/ 40 kHz	1.5 Pa
RF60		60 W		1.4 at.%				
RF80		80 W		4.3 at.%				
RF100		100 W		7.0 at.%				

2.2. Material Characterization

Using atomic force microscopy (AFM, Nanosurf AG, Liestal, Switzerland) in tapping mode, the three-dimensional topography and surface roughness (10 μm × 10 μm) of the film were obtained. To minimize experimental error, measurements were taken at five randomly selected locations. Field emission scanning electron microscopy (FESEM, Verios G4 UC, Thermo Fisher Scientific, Hillsboro, OR, USA) was used to observe the surface and cross-sectional morphology of the film. The elemental composition and content of the Cr-C film on the silicon substrate were analyzed using EDS (Energy Dispersive Spectroscopy) integrated with FESEM. Raman spectroscopy (DXRxi, Thermo Fisher Scientific, Waltham, MA, USA, laser wavelength 532 nm) was used for Raman characterization of the DLC films on the rubber surface. X-ray photoelectron spectroscopy (XPS, Axis Supra, Kratos Analytical Ltd., Manchester, UK) used Al Kα radiation (characteristic energy = 1486.8 eV) as the excitation source to analyze the elemental composition and chemical bonding states of the DLC films on the rubber surface.

To measure the Cr doping content in the Cr-C layer, single-crystal silicon wafers were used as the substrate for EDS analysis. As a high-molecular polymer, ACM rubber has an extremely high carbon content. Direct EDS analysis on the rubber substrate would result in

overlap between the carbon signal from the substrate and that from the Cr-C film. Since the electron beam detection depth of EDS typically ranges from 1 to 2 μm, which may exceed the interlayer thickness, it becomes impossible to accurately calculate the atomic ratio of Cr/C. Therefore, to avoid this interference and ensure the accuracy of the compositional analysis, this study used single-crystal silicon substrates as the reference material. The low carbon content of the silicon substrate helps reduce signal interference, making the elemental measurement results more reliable.

Contact angle (CA) measurements were performed at room temperature using a contact angle tester (JC2000, Powereach, Shanghai, China) with the hanging drop method. To minimize the influence of droplet weight, a minimal droplet volume of 1 μL was maintained. Two liquids were selected for the material evaluations: non-polar CH_2I_2 and polar H_2O. Contact angle values were recorded 15 s after droplet deposition. Solid surface energy (γ_S) and its polar (γ_S^P) and dispersive (γ_S^d) components were calculated using the Owen–Winter–Labelle–Kellogg (OWRK) method [18]. Each liquid surface combination was measured three times to reduce uncertainty.

To determine the interfacial adhesion between the Cr-C/DLC film and the ACM substrate, a qualitative assessment was conducted using the X-Cut method [4,19,20]. The specific procedure for the X-Cut method is as follows: a sharp blade is used to make a distinct "X" shaped cross-incision on the film surface with consistent pressure. The incision depth must ensure complete penetration through the film to reach the substrate. Subsequently, specialized adhesive tape is applied over the incision area and subjected to a constant pressure of approximately 10 N to ensure strong adhesion between the tape and the film surface. After allowing the adhesion to stabilize for 10 min, the tape is rapidly peeled off at a constant speed and specific angle. Finally, SEM is employed to observe the microstructure of the X-Cut area. Qualitative evaluation of the film's interfacial adhesion is performed by comparing the degree of delamination, curling, or fragmentation at the incision edges and surrounding areas. In addition, a scratch tester (CETR-UMT, Bruker, Billerica, MA, USA) equipped with a diamond indenter with a radius of 12.5 μm was used to numerically evaluate the bonding strength of the Cr-C/DLC films on the ACM rubber surface. Under increasing loading conditions, the scratch indenter moved at a rate of 25 μm/s. Within 120 s, the load linearly increased from 0.01 N to 1 N, and the scratch length was 3 mm. The critical load force corresponding to the friction abrupt change was used to calculate the magnitude of the adhesion.

The nanoindentation hardness of the rubber surface film was tested using a nanoindenter (CETR-UMT, Bruker, Billerica, MA, USA) equipped with a Berkovich diamond indenter. The load was linearly increased from 0 to 1 mN over 15 s, followed by a 10 s creep process and a 15 s unloading process. When unloading to 0.1 mN, the thermal drift process was set to 45 s. Five indentation points were taken at each sample location across five distinct regions, with 20 μm spacing between points to avoid residual stress effects from adjacent indentations. Film hardness and elastic modulus were calculated using the Oliver–Pharr method [21].

The tribological properties of the DLC coating on the rubber surface were evaluated using a ball-on-disk tribometer (CETR-UMT, Bruker, Billerica, MA, USA). The test used a commercially available zirconia ball with a diameter of approximately 6 mm as the counter-wear member under a load of 0.3 N. Friction test parameters were as follows: rotational speed of 100 rpm, friction radius of 4 mm, and a test duration of 60 min. An optical microscope was used to observe the wear track morphology of the film and the wear scar morphology of the abrasive ball, while Raman spectroscopy was employed for further analysis. Wear mass loss of the samples before and after the friction test was measured using a balance (LabX ready, XSE 105) (measured three times), yielding wear volume data.

In addition, a stylus profiler (Detak-XT, Bruker, Billerica, MA, USA) was used to scan and measure the width and depth of the wear track. The wear rate K of the samples was obtained through Equations (1) and (2).

$$K = V/(F \times L) \quad (1)$$

$$V = A \times D \quad (2)$$

where K is the wear rate, V is the wear volume, F is the load, and L is the total length of the moving path. A is the cross-sectional area of the wear track, and D is the length of the wear track.

3. Results and Discussion

3.1. Surface and Cross-Section Morphology

Figure 1 shows the surface morphology of Cr-C/DLC films deposited on ACM rubber substrates. Observations reveal that all the prepared films exhibit randomly distributed cracks on their surfaces [22]. This is due to temperature variations during the film deposition process and the difference in thermal expansion coefficients between the DLC film and the rubber substrate. Cracks originate from the initial atomic layers of the DLC coating and propagate upwards, ultimately resulting in micrometer-scale cracks [17]. To investigate the origin of the cracks, Figure S1 shows a rubber sample with only the RF80 Cr-C layer deposited on the ACM rubber surface (without the top-layer DLC). The results indicate that similar random micro-cracks appeared during the deposition of the Cr-C layer. This confirms that the cracks primarily result from thermal effects during the deposition process and the large difference in the coefficient of thermal expansion between the film and the rubber substrate. The deposition of the top-layer DLC continues to extend along these initial paths, ultimately forming a more closely knit network structure. For hard DLC films, the formation of cracks helps enhance flexibility and relieve stress in the film. When the rubber deforms, the film can stretch, thus preventing large-scale brittle peeling [23,24]. As the RF power of the Cr target increases from 40 W to 100 W (corresponding to a rise in Cr content from 0.8 at.% to 7.0 at.%), the surface undulation of the films gradually decreases. This is attributed to the fact that as the Cr content increases, more Cr atoms form bonds with carbon. These atoms first accumulate along the pits on the rubber surface, filling the surface pores. This effectively masks the original defects of the substrate and promotes a smoother surface on the sample. Additionally, the film exhibits a granular structure composed of fine particles. With increasing Cr content, all samples display a "cauliflower-like" granular morphology, indicating that Cr doping does not alter the growth pattern of the carbon-based film. This dense spherical granular structure, combined with stress release through network-like cracks, provides excellent mechanical stability for the Cr-C/DLC film on the rubber substrate.

To systematically investigate the variation in surface roughness of ACM rubber, the surface morphology of the Cr-C/DLC film on the ACM surface was characterized using AFM, as shown in Figure 2. In the stage of relatively low RF power (40 W–80 W), SEM observations indicate that the surface depressions are filled, and the overall surface becomes smoother. Corresponding AFM data show that the Sa value decreases from 280 nm to 207 nm. This reduction may be attributed to the increased kinetic energy and flux of sputtered atoms at higher RF power. Cr and C atoms preferentially deposit and fill the micro-pores and grooves on the rubber surface [25], acting as physical leveling agents that reduce macroscopic undulations. Martinez et al. [14] suggest that the deposition of DLC films on elastic substrates may result in increased roughness due to reticular cracks or a "wrinkling" effect caused by thermal stress. The results of this study indicate that

the synergistic effects of film thickness, substrate pretreatment, and the doping process can effectively suppress this roughening tendency. However, when the power is further increased to 100 W (with a Cr content of 7 at.%), SEM reveals an increase in particle size, and the corresponding AFM measurement results show a rebound of the Sa value to 234 nm. This is attributed to the enhanced collision frequency between atoms in the plasma environment at high power, which causes the Cr-C clusters to agglomerate to some extent before reaching the substrate and deposit on the film surface as larger particles. Dai et al. [26] found that the increase in surface roughness of Cr-DLC films is attributed to the formation of a large amount of CrC due to the rise in chromium content. This finding aligns with the coarsening trend observed via SEM, collectively revealing the regulatory mechanism of Cr doping concentration on film growth patterns.

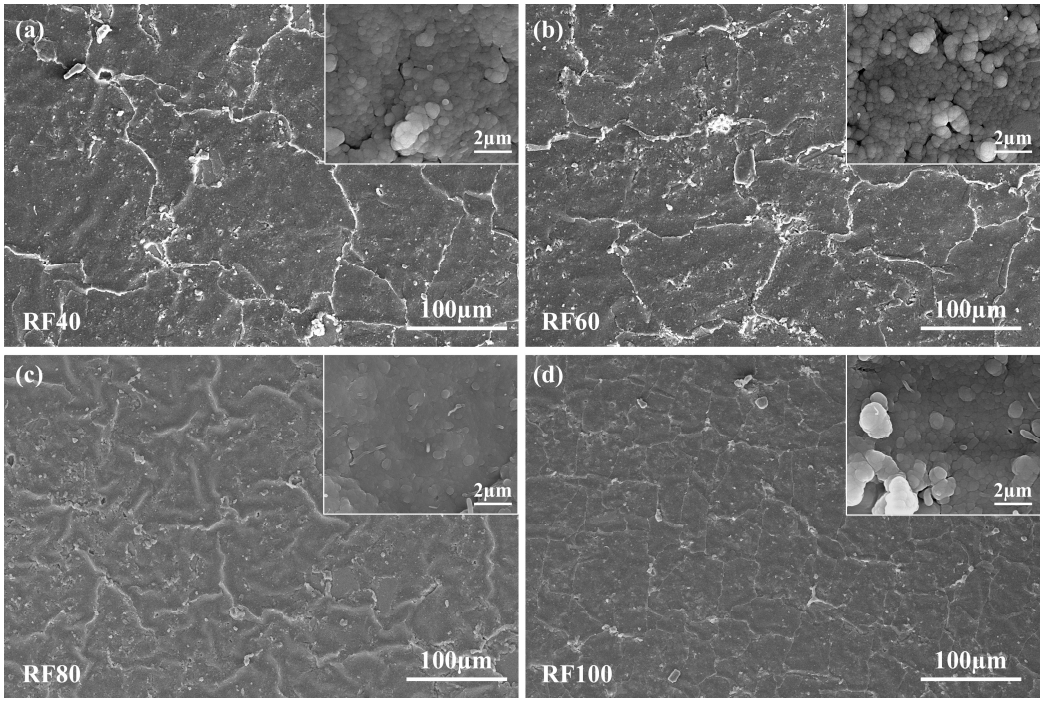


Figure 1. SEM images of Cr-C/DLC films on ACM rubber surfaces: (**a**) RF40, (**b**) RF60, (**c**) RF80, (**d**) RF100.

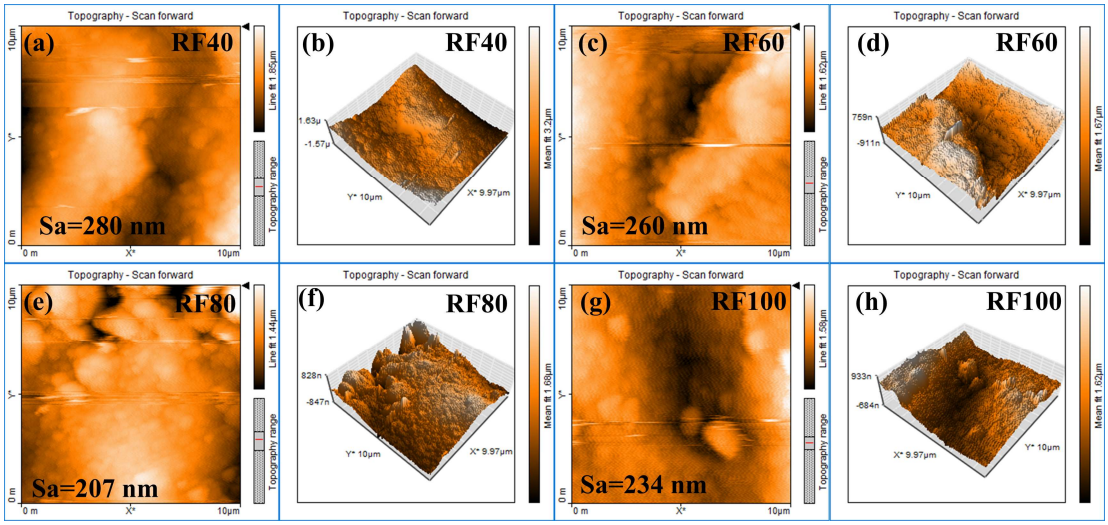


Figure 2. AFM results of Cr-C/DLC films coated on ACM rubber surfaces: (**a**,**b**) RF40, (**c**,**d**) RF60, (**e**,**f**) RF80, (**g**,**h**) RF100.

Figure 3 shows the cross-sectional SEM images of various Cr-C/DLC films deposited on the ACM surface. It can be observed that the film surface is uneven and relatively rough. This is because the surface of the ACM rubber is rough, causing the film deposited on the ACM surface to undulate [27]. The SEM results indicate that an increase in RF sputtering power has little effect on the film thickness. Specifically, when the RF power is in the range of 40 W to 100 W, the total film thickness remains stable in the range of 350 nm to 400 nm with minor fluctuations. Observation of the cross-sectional SEM images reveals no distinct physical boundary or delamination between the Cr-C interfacial layer and the DLC top layer, indicating a strong interfacial bond. Figure 4 shows the EDS mapping corresponding to the SEM cross-sectional morphology of RF100. Only partial accumulation of Cr elements was observed on the surface of the rubber substrate, and no distinct boundary was detected. Moreover, Xu et al. [10] deposited Cr/Cr-C/DLC films and found that the boundary between the Cr-C and DLC layers was indistinct in the EDS mapping of TEM images. This is consistent with the findings of the present study. Therefore, the Cr-C/DLC film in this study is referred to as a "composite film". In addition, since the thickness information of each layer could not be clearly observed in the SEM cross-sectional images of the films and the corresponding EDS mapping, a profilometer was used to measure the step height of the Cr-C intermediate layers and the top DLC film on the silicon wafer surface to obtain the thickness information of each layer. Lubwama et al. [23] pointed out that under the same process parameters, the thickness of the films observed on the rubber surface via SEM is similar to that on the silicon wafer surface. The minor differences may be due to the relatively rough surface of the rubber substrate. The thicknesses of the layers in various samples are shown in Table S1.

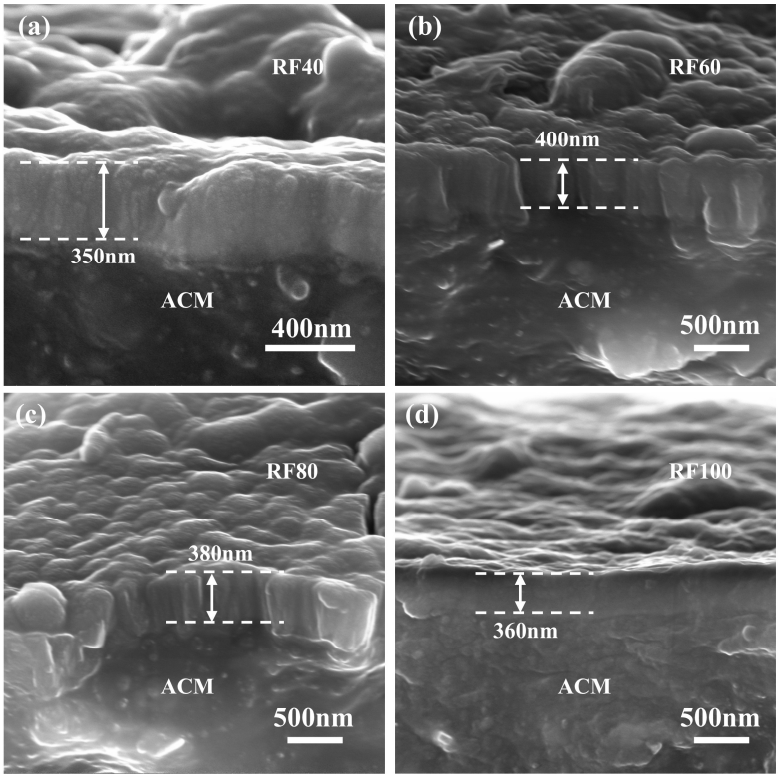


Figure 3. Cross-sectional SEM images of different Cr-C/DLC films deposited on the ACM surface: (**a**) RF40, (**b**) RF60, (**c**) RF80, (**d**) RF100.

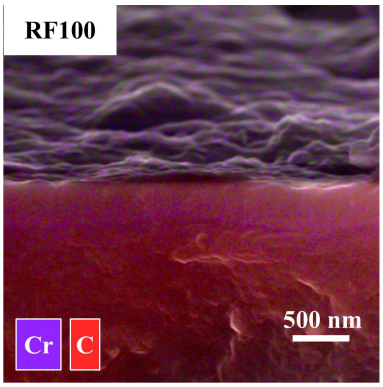


Figure 4. EDS mapping of the cross-sectional SEM image of RF100.

3.2. Composition and Structure of Films

Figure 5 shows the Raman spectra of Cr-C/DLC films with varying Cr doping amounts on the ACM surface. All samples (Figure 5a) exhibit two prominent Raman peaks, namely the D peak at 1350 cm^{-1} and the G peak at 1580 cm^{-1}, which are typical characteristics of DLC films. The D peak is associated with the breathing vibration of sp^2-hybridized carbon atoms in aromatic rings, while the G peak corresponds to the stretching vibration of sp^2-hybridized carbon atoms in graphite chains [28,29]. The I_D/I_G ratio, the position of the G peak ($G_{position}$), and the full width at half maximum of the G peak (G_{FWHM}) are important parameters that provide information on the internal chemical bond structure of the film [30]. Typically, a higher I_D/I_G ratio indicates an increase in the content of sp^2 bonds. As the RF sputtering power increases, the I_D/I_G ratio rises from 1.56 to 1.94, indicating that Cr doping increases the proportion of sp^2 bonds in the film. Furthermore, the $G_{position}$ shifts towards higher wavenumbers and the G_{FWHM} decreases. This further indicates that the content of sp^3 bonds (diamond-like structure) in the film decreases, while the proportion of sp^2 bonds (graphite-like structure) increases.

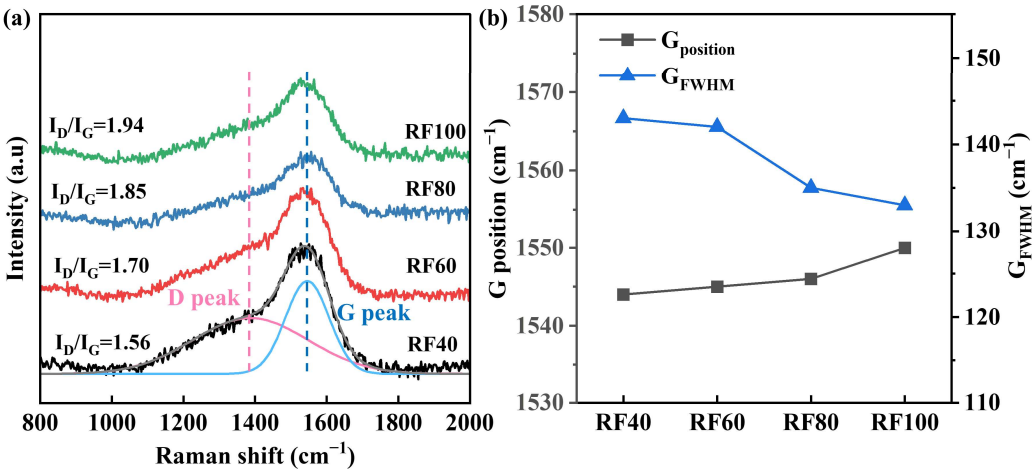


Figure 5. Raman spectra and Gaussian fitting results of Cr-C/DLC films with different Cr doping levels on ACM surfaces: (**a**) Raman spectra; (**b**) $G_{position}$ and G_{FWHM}.

To investigate the elemental composition and chemical bonding characteristics of Cr-C/DLC films, XPS spectral analysis was conducted on RF40, RF60, RF80, and RF100. Figure 6 shows the full XPS spectra, C 1s fine spectra, and sp^2/sp^3 ratios for various Cr-C/DLC films. As shown in Figure 6a, all samples exhibit distinct C 1s peaks near 284.6 eV and O 1s peaks near 531.9 eV, confirming the presence of a carbon film on their surfaces. Each DLC film yielded four peaks from Gaussian type fitting of the C 1s spectrum: a C=C sp^2 bond with a binding energy of 284.5 ± 0.2 eV, a C-C sp^3 bond at 285.2 ± 0.2 eV, a C-O

bond at 286.5 ± 0.2 eV, and a C=O bond with a binding energy of 288.4 ± 0.2 eV [27,31]. The incorporation of chromium increases the peak area corresponding to sp^2 bonds in the film while decreasing that of sp^3 bonds. Figure 6c shows that as the Cr doping concentration increases, the sp^2/sp^3 ratio also rises. He et al. [17] deposited DLC films using the same process parameters and found that variations in interlayer thickness influenced the internal stress of the film, which in turn altered the structure of the top-layer DLC film. Xu et al. [10] confirmed that changes in the intermediate layer directly influence the sp^2 and sp^3 bonding structures in the top-layer DLC film. In addition, Zou et al. [32] observed that in Cr-DLC films with different Cr doping levels, the incorporation of Cr elements weakens the carbon network's compactness, promoting the transformation of sp^3 bonds into sp^2 bonds. Therefore, it is hypothesized that in this study, the variation in Cr doping concentration within the Cr-C interlayer induces changes in the interlayer structure, which is the primary cause of the structural transformation in the top-layer DLC film.

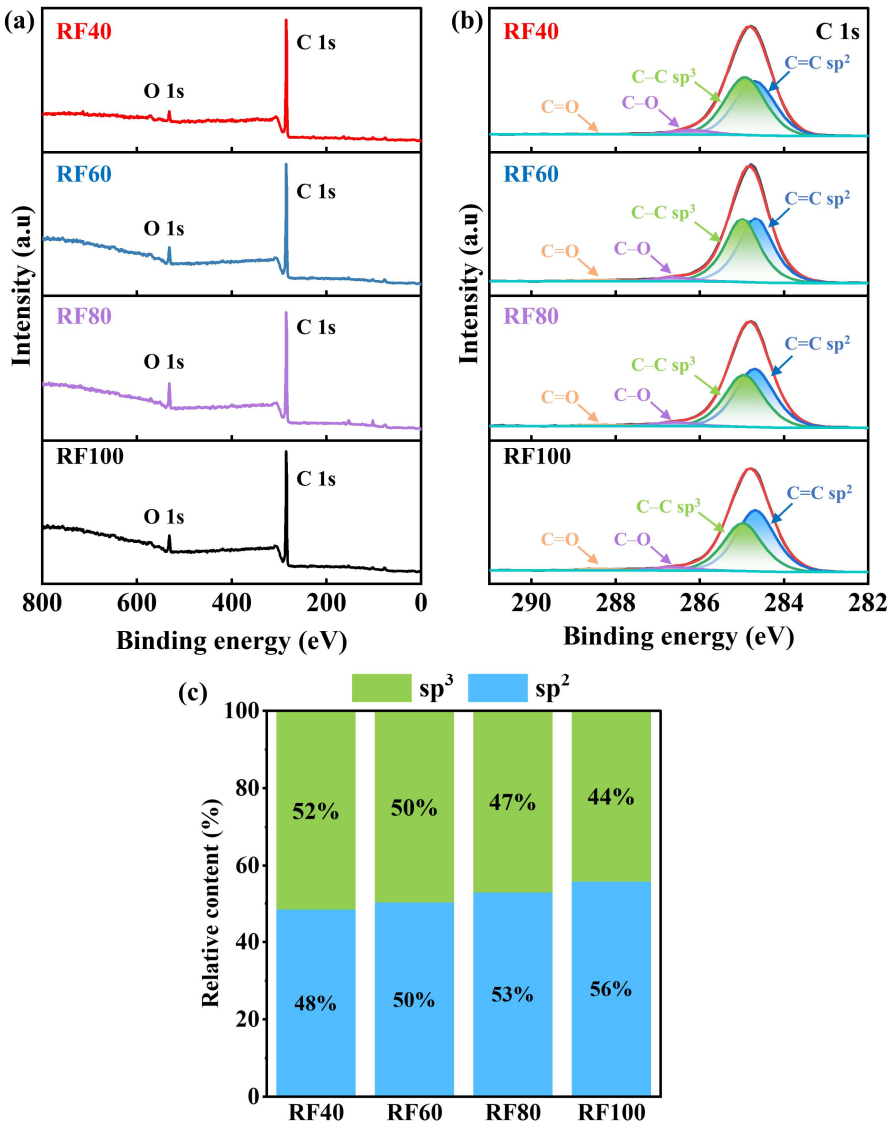


Figure 6. XPS spectra of various Cr-C/DLC films on ACM rubber surface: (**a**) full spectrum, (**b**) C 1s, (**c**) sp^2/sp^3.

3.3. Contact Angle and Surface Energy of Films

Surface wettability is a key indicator for assessing the interface properties of films. Figure 7a shows the contact angle (CA) image of the RF80 sample, exhibiting a static water

contact angle (WCA) of 111.5° ± 1.5°, demonstrating significant hydrophobic characteristics. Figure 7b further illustrates the variation trends of the contact angle (CA) of the film at different RF powers when water and diiodomethane are used as test liquids. The results reveal that the WCA of the pristine ACM rubber and all Cr-C/DLC film samples exceed 90°, primarily attributed to the dense amorphous carbon network of the DLC films and their low surface free energy. As the RF power increased from 40 W to 80 W, the water contact angle gradually increased, peaking at 111.5° ± 1.5° at 80 W (Cr content 4.3 at.%). This trend closely correlates with the surface roughness changes observed via AFM, as described earlier. According to the Wenzel model, for inherently hydrophobic surfaces, a moderate reduction in microscopic roughness (such as that achieved by the RF80 sample) typically corresponds to an increase in the contact angle. This indicates that surface smoothing enhances the hydrophobicity of the film. When the power was further increased to 100 W, surface roughness increased due to particle clustering, resulting in a slight decrease in the water contact angle. However, it remained significantly higher than that of the original ACM substrate, demonstrating the effectiveness of the Cr-C/DLC film in enhancing the hydrophobic stability of the rubber surface.

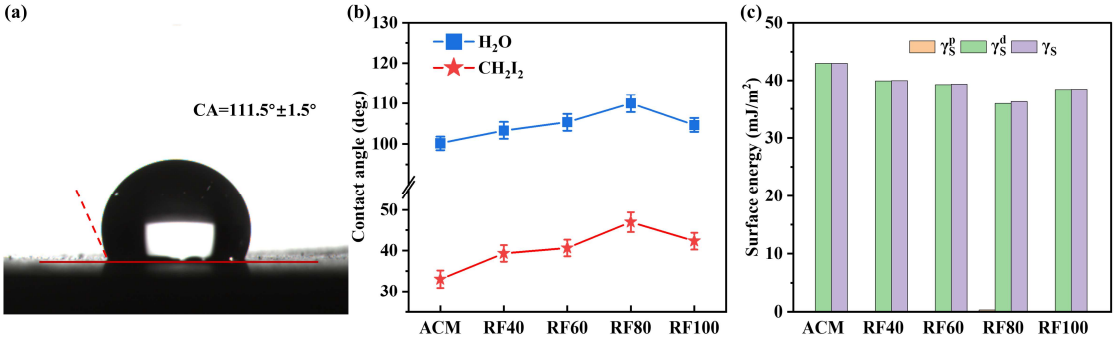


Figure 7. (**a**) Water contact angle images of the RF80 sample, (**b**) water contact angle and diiodomethane contact angle of each sample, (**c**) surface energy of each sample.

Figure 7c shows that the OWRK method was employed to calculate the total surface energy of each sample, along with its dispersion and polarity components. The results indicate that radiofrequency power significantly affects surface energy. As power increases, total surface energy first decreases and then increases, reaching a minimum of 36.25 mJ/m^2 at 80 W. Furthermore, the wettability of DLC films is closely associated with the sp^2/sp^3 ratio on their surface [33]. A surface rich in sp^2 bonds reduces the polar component of the surface energy by decreasing dangling bonds, thus creating a hydrophobic effect [34]. As indicated by Raman spectroscopy and XPS analysis, variations in the Cr doping amount affect the ratio of sp^2 and sp^3 bonds in the DLC film. With an increase in Cr content, the sp^2 content rises, which may contribute to enhancing the hydrophobicity of the coating. Consequently, this slightly increases the contact angle and modifies the surface free energy. Given that the surface free energy is jointly determined by polar and non-polar components, changes in the sp^2/sp^3 ratio can directly impact the non-polar component of the surface energy, thereby altering the contact angle and surface energy of the film. Notably, across all samples, the dispersion component (γ_S^d) dominates the total surface energy (γ_S), with its value remaining nearly equivalent to the total surface energy. In contrast, the polar component (γ_S^P) consistently remains at an extremely low level (approaching 0). This indicates that the interfacial wetting behavior of Cr-C/DLC films on ACM is primarily governed by non-polar van der Waals forces (dispersion forces) rather than interactions involving chemically polar functional groups. This low-polarity characteristic helps re-

duce the affinity between the film and polar media (such as water or certain lubricant components), thereby effectively minimizing adhesive wear during friction processes.

3.4. Adhesion Strength of the Films

Adhesion strength is a key metric for assessing the service reliability of DLC films on rubber substrates. The bond strength of the films was assessed qualitatively using the X-Cut method. This study employed the X-Cut method combined with tape peel tests to qualitatively assess the adhesion strength of Cr-C/DLC films with varying Cr contents. The microstructures observed after peeling are presented in Figure 8. The RF40 sample exhibits significant delamination at the X-section, with large film fragments adhering around the X-Cut (circled in Figure 8a), indicating poor interfacial adhesion. In contrast, the X-Cut surfaces of the RF60 and RF100 samples showed minor flaking of film fragments on both sides. Compared to RF40, the adhesion strength of the RF60 and RF100 samples showed a slight improvement. Notably, the RF80 sample (Cr content 4.3 at.%) demonstrated excellent adhesion stability. Its X-Cut edges remained clean and even, exhibiting only minimal micro-flaking, with no significant film curling observed. This may be attributed to the moderate doping of Cr atoms, which induces an increase in the size of sp^2 atomic clusters within the amorphous carbon network, along with their ordered rearrangement. The transformation of the sp^2 structure effectively alleviates the substantial residual compressive stress accumulated within the film. Wang et al. [35] found that Cr doping effectively alleviates the average internal stress in DLC films, thereby improving the elevated internal stress in DLC films with high sp^3 carbon content. Furthermore, the presence of the Cr-C interlayer reduces the mechanical discontinuity between the hard film and the flexible substrate, allowing for a smooth transition of interfacial stress. This facilitates the suppression of film delamination through the cooperative deformation of random cracks when subjected to mechanical shear forces.

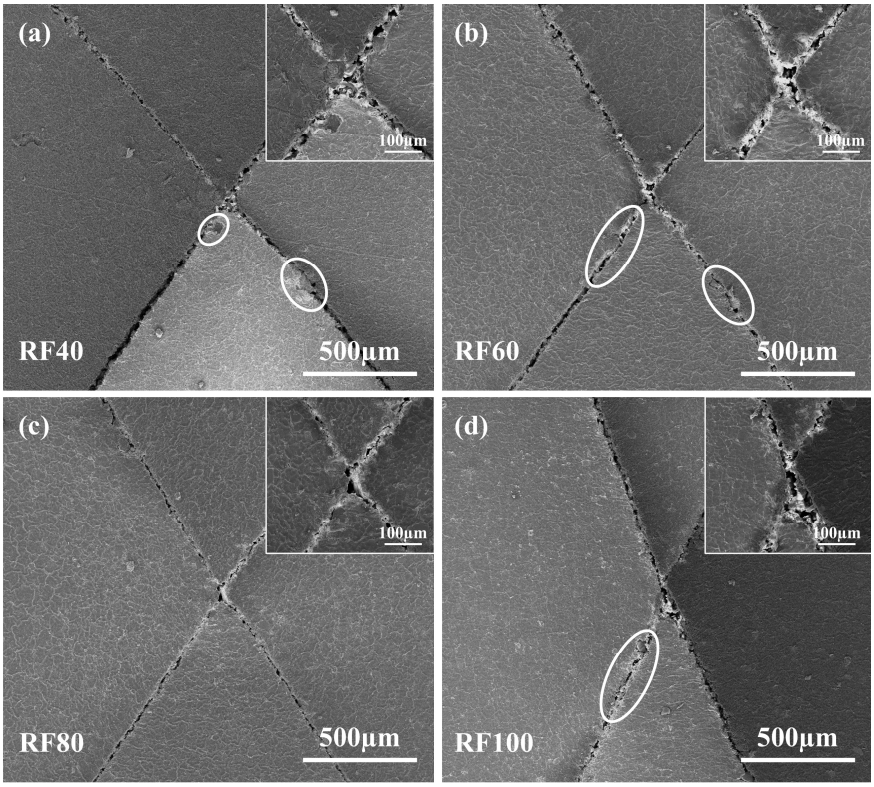


Figure 8. SEM images of X-Cut positions for various Cr-C/DLC films after peel testing: (**a**) RF40, (**b**) RF60, (**c**) RF80, (**d**) RF100.

The qualitative evaluation above could not adequately measure the subtle changes in the adhesion of different Cr-C/DLC films. Therefore, the adhesion of the different films on the rubber surface was further analyzed using the scratch method. The scratch curves of the Cr-C/DLC films deposited on the ACM rubber surface are shown in Figure 9. During the scratch test, two abrupt changes occurred in the friction process, corresponding to changes in the load. The first abrupt change L_{C1} (lower critical load) led to film rupture, while the second abrupt change L_{C2} (upper critical load) marked the critical load required for the film to peel off from the ACM rubber surface. For the films coated on the ACM rubber surface, as the RF power and Cr doping content increased, the adhesion between the Cr-C/DLC films and the ACM rubber first increased and then decreased. Notably, the critical load of the RF80 sample is 1.5 times that of the RF40 sample, which intuitively indicates that the RF80 sample has more excellent adhesion, consistent with the results measured by the X-Cut method.

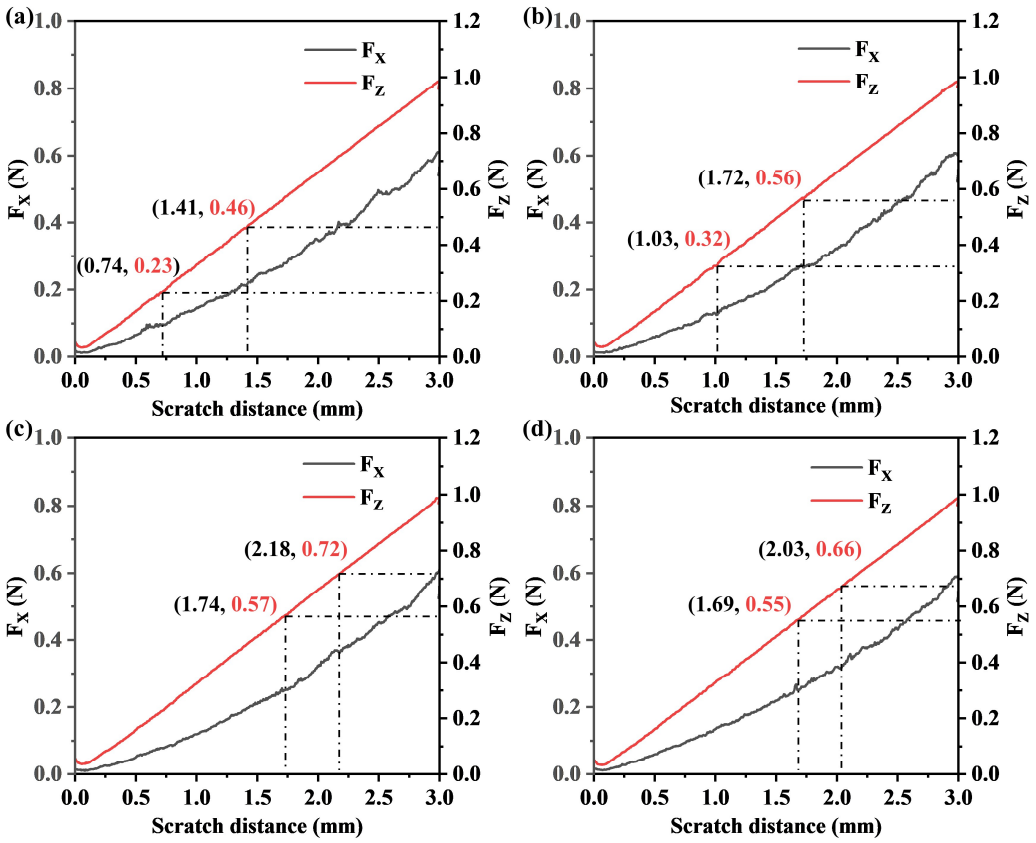


Figure 9. Scratch curves of different Cr-C/DLC films on the ACM rubber surface: (**a**) RF40, (**b**) RF60, (**c**) RF80, (**d**) RF100.

3.5. Mechanical Properties of the Films

Hardness is a critical physical parameter for evaluating the mechanical properties of DLC films. In this experiment, a nanoindenter was used to measure deformation by applying and releasing load on the DLC film surface via the indenter. The entire process was divided into three stages: loading, holding, and unloading. Load and displacement changes were recorded, and the film's hardness and elastic modulus were calculated using the Oliver–Pharr method [36]. Since ACM rubber is a highly elastic material, contact between the indenter and the rubber substrate causes viscoelastic deformation, and the indenter experiences creep during the holding period. Therefore, the measured hardness and elastic modulus are closely related to the holding time, maximum applied load, and unloading rate [37]. Additionally, after the indenter is unloaded, a relatively large indentation depth in

the micrometer range is observed. Qian et al. [38] suggested that when the nanoindentation depth of polymer materials is greater than 800 nm, the errors in the physical quantities of elastic modulus and hardness calculated by the Oliver–Pharr method are relatively small. Figure 10a shows the typical indentation load–depth curves of different Cr-C/DLC films and ACM on the ACM rubber surface. It can be observed that the indentation depth of each Cr-C/DLC film exceeds the total thickness of the film. Thus, the measured hardness is a composite value of the ACM rubber substrate and the Cr-C/DLC film. In industrial seal applications, the film and substrate usually work together, making the composite hardness of the film of practical significance. Moreover, as observed from Figure 10a, as the power increases, the maximum indentation depth h_{max} first decreases and then increases. This indicates that the Cr-C/DLC films under different RF powers have different response mechanisms to the applied load.

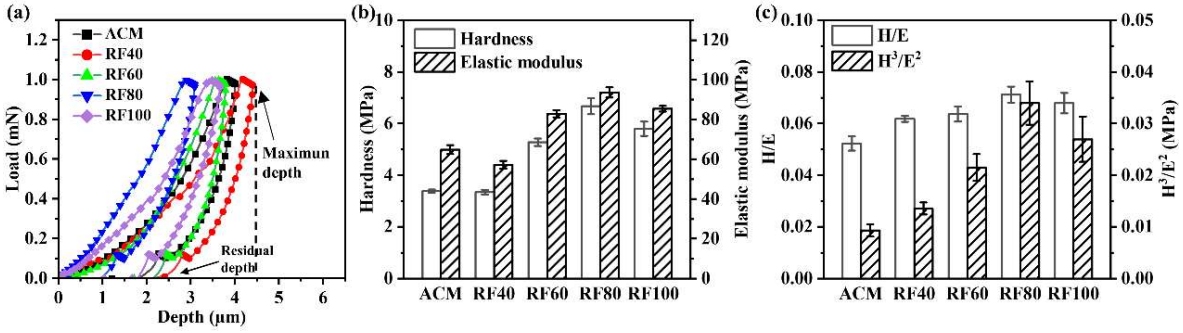


Figure 10. Mechanical properties of different DLC films: (**a**) load–depth curves of various Cr-C/DLC films on ACM rubber surfaces, (**b**) hardness and elastic modulus, (**c**) H/E and H^3/E^2.

Figure 10b shows the changes in hardness and elastic modulus of Cr-C/DLC films deposited on ACM substrates at different RF sputtering powers. As the RF sputtering power increases, the film's hardness and elastic modulus first increase, then decrease. At an RF power of 80 W, the film exhibits a maximum hardness of 6.8 MPa. This is likely due to the high hardness of metallic chromium and the carbides formed by chromium bonding within the carbon-based film. This aligns with the conclusion of the report that thin interlayers contribute to enhancing the hardness and toughness of multilayer nanostructures [39]. These carbides, dispersed throughout the carbon matrix, enhance the hardness of the film. Subsequently, as the RF sputtering power increases, the sp3 carbon content in the film decreases, graphitic bonds increase, and diamond-like bonds decrease, which reduces the film's hardness and elastic modulus. Additionally, the increase in RF sputtering power (100 W) may lead to the formation of a large amount of CrC phase, which could disrupt the continuity of the carbon network structure [40,41]. This is one of the reasons for the reduced hardness of the film. Figure 10c shows the H/E and H^3/E^2 values, which represent the film's resistance to crack initiation and plastic deformation, respectively [42,43]. The results indicate that as the RF sputtering power increases, the H/E and H^3/E^2 values initially rise before subsequently decreasing. This phenomenon can be attributed to the fact that appropriate RF sputtering power facilitates a smooth transition between ACM and Cr-C/DLC, thereby endowing the RF80 film with remarkable toughness and resistance to plastic deformation, which reduces the risk of brittle fracture.

3.6. Tribological Properties of the Films

Figure 11 presents a comparison of the friction coefficient curves, average friction coefficients, wear mass loss, and wear rates for ACM and Cr-C/DLC films on ACM rubber. As shown in Figure 11a, it can be observed that the coefficient of friction (CoF) of ACM rubber without a coating exhibits a significant and rapid decrease during the initial friction

phase. This may be attributed to the flash temperature increase in the contact area caused by frictional heat generation [44]. As the test progressed, the coefficient of friction gradually stabilized at approximately 0.8, indicating that the friction process had reached a steady state. In contrast, ACM coated with Cr-C/DLC nanocomposite films exhibits varying degrees of friction coefficient reduction, indicating that Cr-C/DLC significantly enhances the tribological properties of ACM rubber. As the RF sputtering power increases, the CoF first decreases and then increases. At 40 W RF, the Cr content is relatively low, and the CoF remains at a low level of approximately 0.18 before 800 s. After this point, due to film detachment, the friction ball contacts the rubber substrate, causing the coefficient of friction to rise sharply. Low concentration Cr doping in the interlayer increases the sp^3 bond content within the film, enhancing its hardness and elastic modulus. However, this fails to adequately mitigate the physical property mismatch between the DLC hard film and the ACM elastic substrate. Under prolonged dynamic operating conditions, the film is prone to delamination and failure, which compromises its wear resistance. After 800 s, the film wears through the ACM substrate, causing a rapid increase in the CoF. As shown in Figure 11b, the average coefficients of friction for RF40, RF60, RF80, and RF100 are 0.23, 0.17, 0.13, and 0.14, respectively. With increasing RF sputtering power and Cr content, the CoF exhibits a trend of first decreasing and then increasing. At an RF power of 80 W, the CoF reaches its minimum value and stabilizes at 0.14. Besides the coefficient of friction, wear mass loss and wear rate are also important indicators of the tribological properties of the film. As shown in Figure 11b, the wear mass loss and wear rate of RF80 remain at the lowest levels, being 0.11 mg and 3.1 × 10^{-4} mm^3/(Nm) respectively. Raman spectroscopy and XPS show that the doping of Cr elements increases the graphitization degree of the film. Therefore, Cr-C/DLC is more likely to form a transfer film during the friction process. Compared with the original ACM rubber, the Cr-C/DLC film exhibits a lower CoF, wear mass loss, and wear rate. This can be attributed to the optimal incorporation of Cr into the interlayer, which enhances the bonding strength between the DLC film and the substrate. This ensures the film's performance under sustained friction and wear conditions, achieving excellent wear resistance with low friction and wear rate.

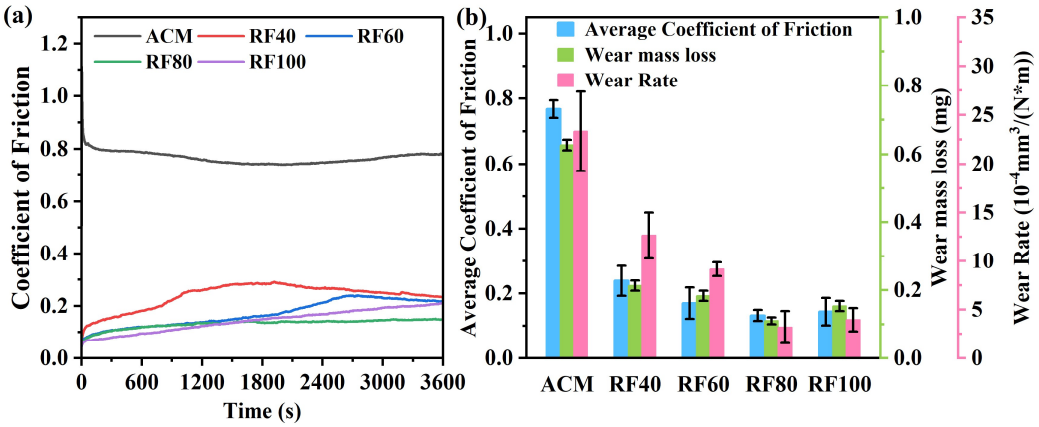


Figure 11. (**a**) Coefficient of friction curves and (**b**) average coefficient of friction, wear mass loss, and wear rate of ACM and Cr-C/DLC on ACM.

Figure 12 shows the wear scar morphology of Cr-C/DLC films prepared at different RF powers after friction testing. The results indicate that as RF power (Cr content) increases, the wear track width first decreases and then increases, reaching a minimum value (~396 μm) at RF 80 W (Cr content 4.3 at.%), demonstrating optimal wear resistance. In the low-power range (RF < 80 W), the scratched surface exhibits roughness and is densely covered with numerous exfoliated particles, indicating severe structural failure of the film. This can

be attributed to insufficient bonding strength at the film/substrate interface under low Cr content, which fails to resist shear stresses during friction. Film fragmentation during friction generates hard particles that contribute to adhesive wear, leading to severe wear. Conversely, when RF power increased to 80 W and 100 W, the wear area appeared polished with no discernible wear marks, and the coating remained adhered to the substrate surface after the friction test. This significant improvement stems from the optimized chromium content (4.3 at.% to 7 at.%) within this range. On one hand, the Cr-C interlayer effectively mitigates interfacial stress concentration, thereby enhancing bonding strength. On the other hand, as discussed earlier regarding mechanical properties, the RF 80 sample exhibits the highest H^3/E^2 ratio, endowing the film with exceptional resistance to plastic deformation. It can be concluded that the Cr content in the interlayer must be maintained within a specific range (4.3 at.% to 7 at.%) to ensure the quality of Cr-C/DLC films, thereby preserving and significantly improving ACM friction performance.

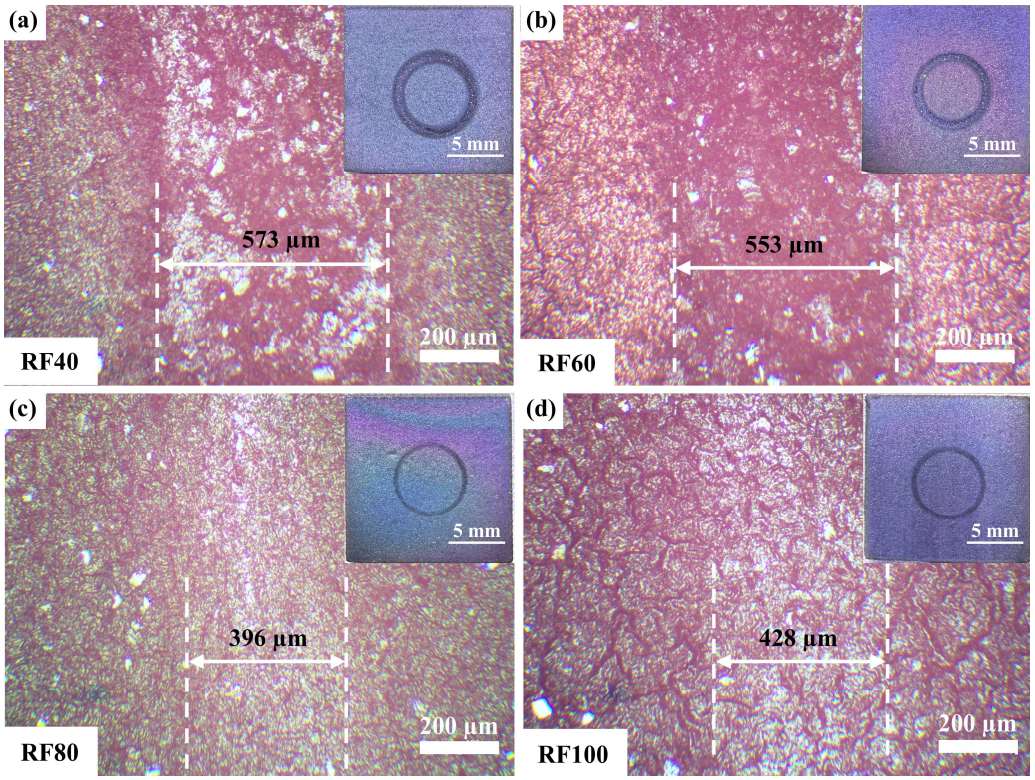


Figure 12. Wear track morphology of Cr-C/DLC films deposited on ACM substrates at different RF sputtering powers: (**a**) RF40, (**b**) RF60, (**c**) RF80, (**d**) RF100.

To further investigate the wear scars of different Cr-C/DLC films on the ACM rubber surface, Raman spectroscopy was used to analyze both the surface and the wear track regions of the DLC films, as shown in Figure 13. It can be clearly seen that, after the friction test, the Raman spectra of the wear track regions of RF40 and RF60 exhibit obvious wavy curves, which are typical Raman signals of polymer materials [45]. This indicates that RF40 and RF60 have failed during the wear process. In contrast, the Raman spectra of the wear scar regions of RF80 and RF100 are similar to those of the corresponding surfaces, with distinct D peaks and G peaks. This is consistent with the results observed in Figure 12, which jointly demonstrate the excellent tribological properties of the RF80 and RF100 samples. In addition, as shown in Figure 14, the Raman signals of the transfer film, namely an indistinct D peak and a distinct G peak, can be clearly observed within the wear scar of the abrasive ball of RF80. This implies that an appropriate amount of Cr doping facilitates

the formation of the transfer film during the friction process, further contributing to the reduction in the friction coefficient.

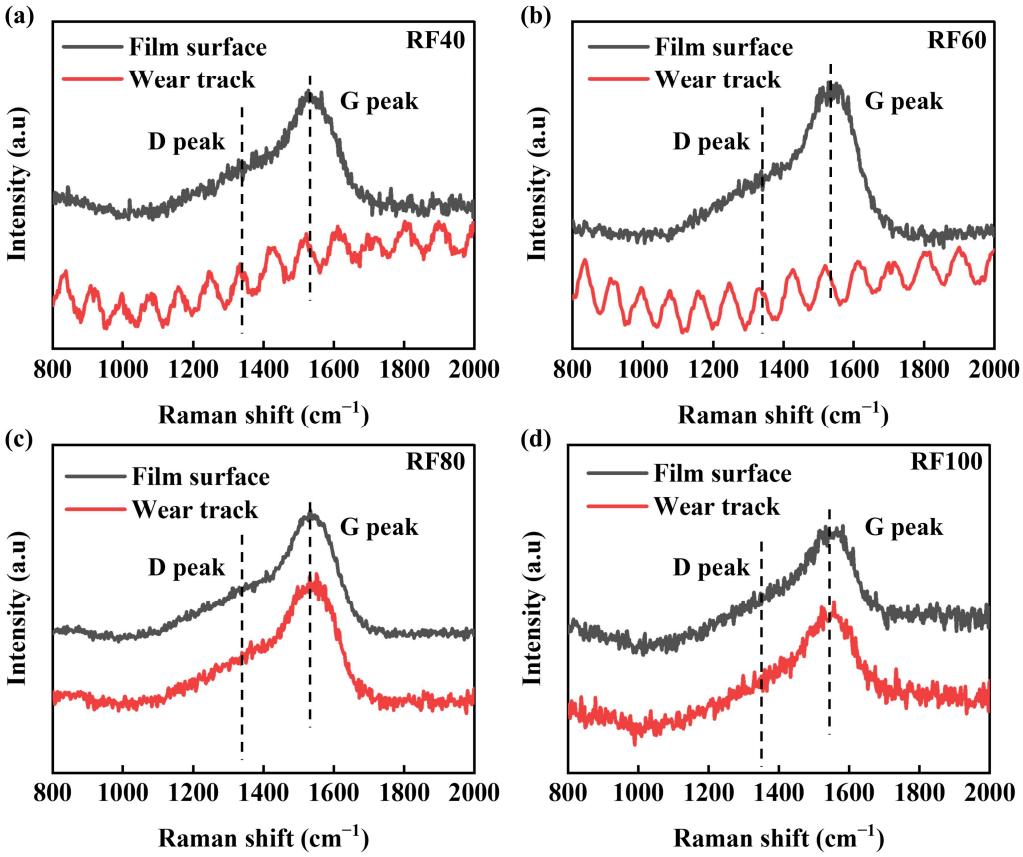


Figure 13. Raman spectra of the wear tracks of various Cr-C/DLC films on the surface of ACM rubber: (**a**) RF40, (**b**) RF60, (**c**) RF80, (**d**) RF100.

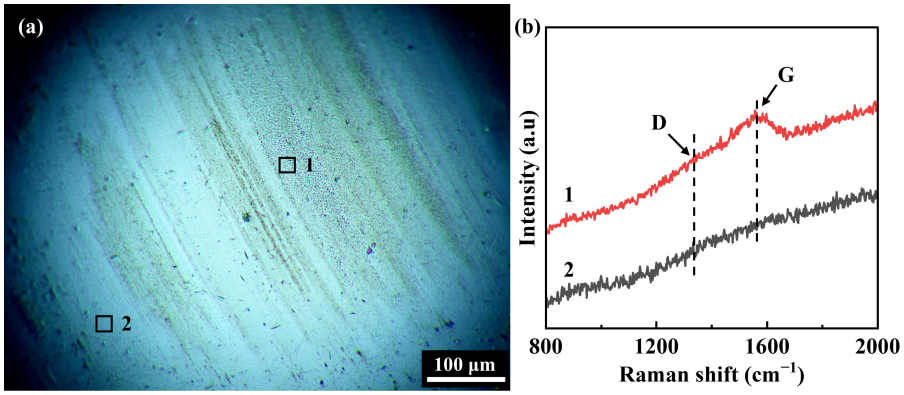


Figure 14. (**a**) Morphology of wear scars corresponding to the RF80 abrasive ball, (**b**) Raman spectra corresponding to the wear scar morphology.

4. Conclusions

This study employed radiofrequency magnetron sputtering (RF-MS) and high-power pulse magnetron sputtering (HiPIMS) for co-sputtering Cr-C layers, successfully fabricating Cr-C/DLC composite films with varying Cr doping levels on ACM rubber substrates. The effects of RF power (Cr doping content) on the films' microstructure, composition, wettability, mechanical properties, and tribological behavior were systematically investigated. The main conclusions are as follows:

(1) Due to the significant difference in the coefficients of thermal expansion between the DLC film and the rubber substrate, a randomly distributed, network-like micro-crack structure appears on the surface of all films. Cross-sectional SEM and corresponding EDS mapping reveal no distinct boundary between the Cr-C interlayer and the top DLC film, suggesting strong interfacial adhesion.
(2) The introduction of the Cr-C interlayer significantly affected the bonding structure of the top-layer DLC film. As the Cr doping content increased, the proportion of sp^2 hybrid bonds also increased. This structural transformation effectively alleviated the residual compressive stress within the film, resulting in stronger film–substrate adhesion during the adhesion test.
(3) The RF80 sample (Cr 4.3 at.%) exhibits excellent mechanical and tribological properties, with a hardness of 6.8 MPa, a friction coefficient of 0.13, and a wear rate of 3.1×10^{-4} $mm^3/(Nm)$. Additionally, moderate Cr doping promoted the formation of a graphite transfer film, resulting in reduced friction and wear.

Supplementary Materials: The following supporting information can be downloaded at: https://www.mdpi.com/article/10.3390/lubricants14040148/s1. Figure S1: SEM image of the Cr-C interlayer of the RF80 sample on ACM rubber; Table S1: Cr-C interlayer thickness and DLC thickness for various films.

Author Contributions: Data curation, K.C. and N.Z.; funding acquisition, H.C. and F.W.; investigation, K.C. and Q.D.; project administration, Q.D., H.C., and F.W.; writing—original draft, K.C.; writing—review and editing, F.W., Q.D., and H.C. All authors have read and agreed to the published version of the manuscript.

Funding: This project was supported by the Hainan Provincial Natural Science Foundation of China (420RC525), Hainan Province Science and Technology Special Fund (ZDYF2019206) and Open Project of State Key Laboratory of Advanced Refractories (Shanghai, No. SKLAR-KF-2025-06).

Data Availability Statement: The original contributions presented in this study are included in the article/Supplementary Materials. Further inquiries can be directed to the corresponding authors.

Acknowledgments: The authors thank the assistance provided by Hainan University Analysis and Testing Center.

Conflicts of Interest: The authors declare no conflicts of interest.

References

1. Dong, C.L.; Yuan, C.Q.; Bai, X.Q.; Yan, X.P.; Peng, Z. Tribological properties of aged nitrile butadiene rubber under dry sliding conditions. *Wear* **2015**, *322*, 226–237. [CrossRef]
2. Su, R.; Liu, G.Y.; Sun, H.G.; Yong, Z.F. A new method to measure the three-dimensional solubility parameters of acrylate rubber and predict its oil resistance. *Polym. Bull.* **2021**, *79*, 971–984. [CrossRef]
3. Mueller, M.; Sleger, V.; Cedik, J.; Pexa, M. Research on the Material Compatibility of Elastomer Sealing O-Rings. *Polymers* **2022**, *14*, 3323. [CrossRef] [PubMed]
4. Xu, Y.; Jia, J.H.; Zhang, G.A.; Li, H.C.; Chen, T.J. Effect of rubber substrates on the flexibility and tribological properties of diamond-like carbon coatings. *Surf. Coat. Technol.* **2021**, *422*, 127526. [CrossRef]
5. Wei, J.; Guo, P.; Liu, L.L.; Li, H.C.; Li, H.; Wang, S.Y.; Ke, P.L.; Saito, H.; Wang, A.Y. Corrosion resistance of amorphous carbon film in 3.5 wt% NaCl solution for marine application. *Electrochim. Acta.* **2020**, *346*, 136282. [CrossRef]
6. Bai, C.; Liang, A.; Cao, Z.; Qiang, L.; Zhang, J. Achieving a high adhesion and excellent wear resistance diamond-like carbon film coated on NBR rubber by Ar plasma pretreatment. *Diam. Relat. Mater.* **2018**, *89*, 84–93. [CrossRef]
7. Zhou, X.; Zhang, Y.; Guo, P.; Cui, L.; Wang, A.; Ke, P. Tribological behavior of Cr/a-C multilayered coating against PEEK under dry sliding condition. *Wear* **2023**, *518*, 204625. [CrossRef]
8. Rajak, D.K.; Kumar, A.; Behera, A.; Menezes, P.L. Diamond-Like Carbon (DLC) Coatings: Classification, Properties, and Applications. *Appl. Sci.* **2021**, *11*, 4445. [CrossRef]

9. Hao, T.M.; Du, J.; Su, G.H.; Zhang, P.R.; Sun, Y.J.; Zhang, J.J. Mechanical and cutting performance of cemented carbide tools with Cr/x/DLC composite coatings. *Int. J. Adv. Manuf. Technol.* **2020**, *106*, 5241–5254. [CrossRef]
10. Xu, Y.J.; Wu, Y.X.; Wang, J.Y.; Zhang, T.; Chen, Y.; Liu, Y. Effect of the Cr/Cr-C sublayer on the adhesional strength and tribological properties of DLC film. *Surf. Coat. Technol.* **2026**, *519*, 132948. [CrossRef]
11. Zhao, L.; Tang, J.; Zhou, M.; Shen, K. A review of the coefficient of thermal expansion and thermal conductivity of graphite. *New Carbon Mater.* **2022**, *37*, 544–555. [CrossRef]
12. Wu, Y.M.; Liu, J.Q.; Cao, H.T.; Wu, Z.Y.; Wang, Q.; Ma, Y.P.; Jiang, H.; Wen, F.; Pei, Y.T. On the adhesion and wear resistance of DLC films deposited on nitrile butadiene rubber: A Ti-C interlayer. *Diam. Relat. Mater.* **2020**, *101*, 107563. [CrossRef]
13. Pei, Y.T.; Bui, X.L.; De Hosson, J.T.M. Deposition and characterization of hydrogenated diamond-like carbon thin films on rubber seals. *Thin Solid Films* **2010**, *518*, S42–S45. [CrossRef]
14. Martinez-Martinez, D.; Schenkel, M.; Pei, Y.T.; Hosson, J.T.M.D. Microstructural and frictional control of diamond-like carbon films deposited on acrylic rubber by plasma assisted chemical vapor deposition. *Thin Solid Films* **2011**, *519*, 2213–2217. [CrossRef]
15. Pei, Y.T.; Bui, X.L.; Zhou, X.B.; De Hosson, J.T.M. Microstructure and tribological behavior of tungsten-containing diamondlike carbon coated rubbers. *J. Vac. Sci. Technol. A* **2008**, *26*, 1085–1092. [CrossRef]
16. Lubwama, M.; Corcoran, B.; Sayers, K.; Kirabira, J.B.; Sebbit, A.; McDonnell, K.A.; Dowling, D. Adhesion and composite micro-hardness of DLC and Si-DLC films deposited on nitrile rubber. *Surf. Coat. Technol.* **2012**, *206*, 4881–4886. [CrossRef]
17. He, Y.; Su, F.H.; Sun, J.F.; Li, Z.J.; Liu, Y.F. Microstructure and tribological properties of DLC films with varying Ti interlayer thicknesses on HNBR substrate deposited by PVD. *Surf. Coat. Technol.* **2025**, *513*, 132515. [CrossRef]
18. Oss, V.; Carel, J. *Interfacial Forces in Aqueous Media*, 2nd ed.; CRC Press: Boca Raton, FL, USA, 2006. [CrossRef]
19. Bai, C.N.; Gong, Z.B.; An, L.L.; Qiang, L.; Zhang, J.Y.; Yushkov, G.; Nikolaev, A.; Shandrikov, M.; Zhang, B. Adhesion and friction performance of DLC/rubber: The influence of plasma pretreatment. *Friction* **2021**, *9*, 627–641. [CrossRef]
20. Qiang, L.; Bai, C.; Liang, A.; Zhang, J. Enhancing the adhesion and tribological performance of Si-DLC film on NBR by Ar plasma pretreatment under a high bias. *Aip Adv.* **2019**, *9*, 015301. [CrossRef]
21. Oliver, W.C.; Pharr, G.M. An improved technique for determining hardness and elastic modulus using load and displacement sensing indentation experiments. *J. Mater. Res.* **1992**, *7*, 1564–1583. [CrossRef]
22. Martinez, L.; Nevshupa, R.; Alvarez, L.; Huttel, Y.; Faverjon, F. Application of diamond-like carbon coatings to elastomers frictional surfaces. *Tribol. Int.* **2009**, *42*, 584–590. [CrossRef]
23. Lubwama, M.; McDonnell, K.A.; Kirabira, J.B.; Sebbit, A.; Sayers, K.; Dowling, D.; Corcoran, B. Characteristics and tribological performance of DLC and Si-DLC films deposited on nitrile rubber. *Surf. Coat. Technol.* **2012**, *206*, 4585–4593. [CrossRef]
24. Pei, Y.T.; Martinez-Martinez, D.; van der Pal, J.P.; Bui, X.L.; Zhou, X.B.; De Hosson, J.T.M. Flexible diamond-like carbon films on rubber: Friction and the effect of viscoelastic deformation of rubber substrates. *Acta Mater.* **2012**, *60*, 7216–7225. [CrossRef]
25. Mousinho, A.P.; Mansano, R.D.; Salvadori, M.C. Influence of substrate surface topography in the deposition of nanostructured diamond-like carbon films by high density plasma chemical vapor deposition. *Surf. Coat. Technol.* **2009**, *203*, 1193–1198. [CrossRef]
26. Dai, W.; Ke, P.; Wang, A. Microstructure and property evolution of Cr-DLC films with different Cr content deposited by a hybrid beam technique. *Vacuum* **2011**, *85*, 792–797. [CrossRef]
27. Qiang, L.; Bai, C.N.; Gong, Z.B.; Liang, A.M.; Zhang, J.Y. Microstructure, adhesion and tribological behaviors of Si interlayer/Si doping diamond-like carbon film developed on nitrile butadiene rubber. *Diam. Relat. Mater.* **2019**, *92*, 208–218. [CrossRef]
28. Casiraghi, C.; Piazza, F.; Ferrari, A.; Grambole, D.; Robertson, J. Bonding in hydrogenated diamond-like carbon by Raman spectroscopy. *Diam. Relat. Mater.* **2005**, *14*, 1098–1102. [CrossRef]
29. Ferrari, A.C.; Robertson, J. Raman spectroscopy of amorphous, nanostructured, diamond-like carbon, and nanodiamond. *Philos. Trans. R. Soc. Lond. Ser. A* **2004**, *362*, 2477–2512. [CrossRef]
30. Ferrari, A.C. Determination of bonding in diamond-like carbon by Raman spectroscopy. *Diam. Relat. Mater.* **2002**, *11*, 1053–1061. [CrossRef]
31. Feng, K.J.; Guo, C.Q.; Lin, S.S.; Fu, Z.Q.; Shi, Q.; Su, Y.F.; Wang, W.; Dai, M.J. Structure and properties of ta-C films prepared by vacuum cathodic arc with an unbalanced external electromagnetic field. *Ceram. Int.* **2022**, *48*, 111–119. [CrossRef]
32. Zou, C.W.; Wang, H.J.; Feng, L.; Xue, S.W. Effects of Cr concentrations on the microstructure, hardness, and temperature-dependent tribological properties of Cr-DLC coatings. *Appl. Surf. Sci.* **2013**, *286*, 137–141. [CrossRef]
33. Sun, L.; Guo, P.; Ke, P.; Li, X.; Wang, A. Synergistic effect of Cu/Cr co-doping on the wettability and mechanical properties of diamond-like carbon films. *Diam. Relat. Mater.* **2016**, *68*, 1–9. [CrossRef]
34. Asl, A.M.; Kameli, P.; Ranjbar, M.; Salamati, H.; Jannesari, M. Correlations between microstructure and hydrophobicity properties of pulsed laser deposited diamond-like carbon films. *Superlattices Microstruct.* **2015**, *81*, 64–79. [CrossRef]
35. Wang, J.; Wang, L.; Chen, H.; Wang, H. Molecular dynamics simulation of friction in DLC films with different Cr doping levels. *Diam. Relat. Mater.* **2024**, *149*, 111612. [CrossRef]
36. Oliver, W.C.; Pharr, G.M. Measurement of hardness and elastic modulus by instrumented indentation: Advances in understanding and refinements to methodology. *J. Mater. Res.* **2004**, *19*, 3–20. [CrossRef]

37. Yang, S.; Zhang, Y.-W.; Zeng, K. Analysis of nanoindentation creep for polymeric materials. *J. Appl. Phys.* **2004**, *95*, 3655–3666. [CrossRef]
38. Qian, Z.; Risan, J.; Stadnick, B.; McKenna, G.B. Apparent depth-dependent modulus and hardness of polymers by nanoindentation: Investigation of surface detection error and pressure effects. *J. Polym. Sci. Part B Polym. Phys.* **2018**, *56*, 414–428. [CrossRef]
39. Robertson, J. Diamond-like amorphous carbon. *Mater. Sci. Eng. R Rep.* **2002**, *37*, 129–281. [CrossRef]
40. Santiago, J.A.; Fernández-Martínez, I.; Sánchez-López, J.C.; Rojas, T.C.; Wennberg, A.; Bellido-González, V.; Molina-Aldareguia, J.M.; Monclús, M.A.; González-Arrabal, R. Tribomechanical properties of hard Cr-doped DLC coatings deposited by low-frequency HiPIMS. *Surf. Coat. Technol.* **2020**, *382*, 124899. [CrossRef]
41. Zheng, J.; Shang, J.L.; Zhuang, W.J.; Ding, J.C.; Mei, H.J.; Yang, Y.; Ran, S.L. Structural and tribomechanical properties of Cr-DLC films deposited by reactive high power impulse magnetron sputtering. *Vacuum* **2024**, *230*, 113611. [CrossRef]
42. Bai, W.Q.; Li, L.L.; Wang, X.L.; He, F.F.; Liu, D.G.; Jin, G.; Tu, J.P. Effects of Ti content on microstructure, mechanical and tribological properties of Ti-doped amorphous carbon multilayer films. *Surf. Coat. Technol.* **2015**, *266*, 70–78. [CrossRef]
43. Fu, Y.Q.; Zhou, F.; Zhang, M.D.; Wang, Q.Z.; Zhou, Z.F. Structural, mechanical and tribocorrosion performances of CrMoSiN coatings with various Mo contents in artificial seawater. *Appl. Surf. Sci.* **2020**, *525*, 146629. [CrossRef]
44. Pinedo, B.; Hadfield, M.; Tzanakis, I.; Conte, M.; Anand, M. Thermal analysis and tribological investigation on TPU and NBR elastomers applied to sealing applications. *Tribol. Int.* **2018**, *127*, 24–36. [CrossRef]
45. Qiang, L.; Yu, S.C.; Liu, G.Q.; Tang, H.L.; Zhang, X.K.; Zhang, J.Y. Comparative study on the influence of bias on the properties of Si-DLC film with and without Si interlayer on NBR: The role of Si interlayer. *Diam. Relat. Mater.* **2020**, *101*, 107614. [CrossRef]

Disclaimer/Publisher's Note: The statements, opinions and data contained in all publications are solely those of the individual author(s) and contributor(s) and not of MDPI and/or the editor(s). MDPI and/or the editor(s) disclaim responsibility for any injury to people or property resulting from any ideas, methods, instructions or products referred to in the content.